Electronic Supplementary Material (ESI) for Materials Chemistry Frontiers.
This journal is © the Partner Organisations 2022

Enhanced photovoltaic output of bifacial perovskite solar cells via tailoring photoelectric balance in rear window layers with 1T-WS_2 nanosheets engineering

Lin Fan,[ab] Wanhong Lü,[a] Wanting Hu,[a] Donglai Han,[c] Shuo Yang,[d] Dandan Wang,[e] Zhihong Mai,[e] Fengyou Wang,[ab] Huilian Liu,[ab] Jinghai Yang,[**ab] and Lili Yang[*ab]

[a] *Key Laboratory of Functional Materials Physics and Chemistry of the Ministry of Education, Jilin Normal University, Changchun 130103, China*

[b] *National Demonstration Center for Experimental Physics Education, Jilin Normal University, Siping 136000, China*

[c] *School of Materials Science and Engineering, Changchun University of Science and Technology，Changchun 130022, China*

[d] *College of Science, Changchun University, Changchun 130022, China*

[e] *Hubei JiuFengShan Laboratory, Future Science and Technology City, Wuhan, Hubei, 420000, China*

E-mail addresses: llyang1980@126.com (Lili Yang), jhyang1@jlnu.edu.cn (Jinghai Yang).

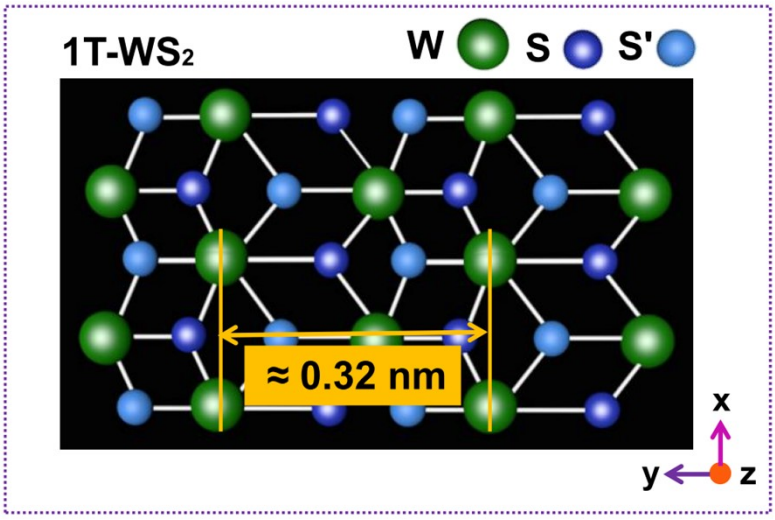

Fig. S1 Top-view molecule structures of 1T-WS_2. W atoms are in green and S atoms are in purple and blue for top and bottom layers, respectively.

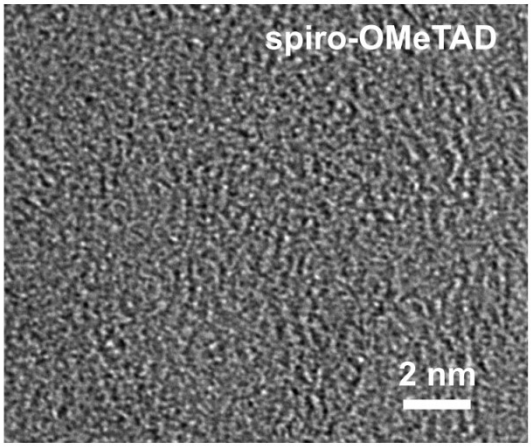

Fig. S2 HRTEM image of spiro-OMeTAD film.

Fig. S3 (a) Raman spectra of SP and SP + W films. (b) Surface SEM image and elemental mappings (W and S) of SP + W film.

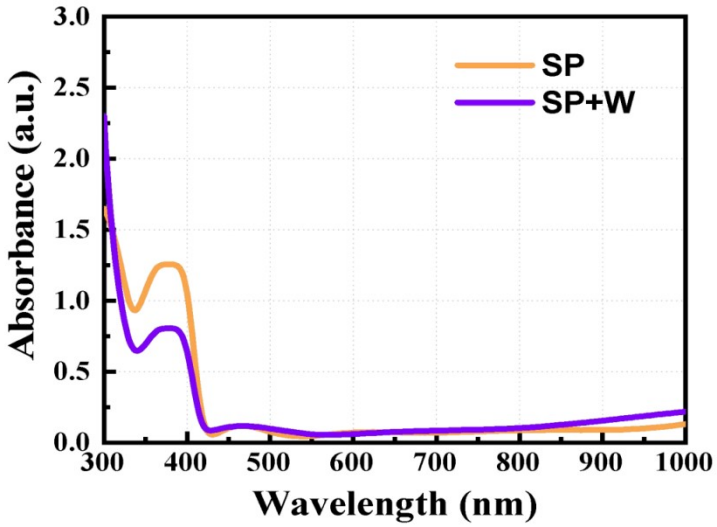

Fig. S4 UV–vis absorption spectra of SP and SP + W films.

Fig. S5 (a) TRPL plots and fitting curves of Glass/PVK/SP and Glass/PVK/SP + W substrates. (b) Nyquist plots of solar cells based on SP and SP + W HTLs, obtained with a bias of 0.8 V in dark. Inset: equivalent circuit used to fit the data.

Fig. S6 (a) OCVD curves and (b) dark-current measurements of the corresponding devices.

Fig. S7 Optimization of the optical and electrical properties of different SP + W films deposited on ITO-glass substrates: (a) transmittance, (b) UV-vis absorption, and (c) conductivity.

Fig. S8 (a) *J*–*V* curves of the best-performing SP-based b-PSC illuminated on different sides. (b) Corresponding EQE spectra and integrated J_{SC} .

Fig. S9 Steady-state current densities measured at the voltage of the maximum power point for (a) SP and (b) SP + W b-PSCs.

Table S1 Hall measurement results of SP and SP + W films

Samples	Conductivity	Resistivity	Hall Mobility	Thickness

	(S/cm)	(Ω·cm)	(cm^2/V·s)	(nm)
SP	5.00×10^{-7}	2.00×10^{6}	3.57×10^{-3}	~ 230 nm
SP + W	6.57×10^{-5}	1.50×10^{4}	6.04×10^{-3}	~ 150 nm

Table S2 Fitting parameters from EIS

Samples	R_s (Ω)	R_{tr} (Ω)	R_{rec} (Ω)	C_{tr} (F)	C_{rec} (F)
SP	34.21	24.66	383.3	7.3×10^{-9}	5.6×10^{-9}
SP + W	27.86	18.81	468.3	7.1×10^{-9}	6.4×10^{-9}

Experimental section

***Materials and reagents*:**

Etched indium-doped tin oxide (ITO, 2 × 2 cm^2) conducting glasses were purchased from Yingkou Optimum Trade Co., Ltd., whereas tin oxide colloidal dispersion (SnO_2 15% in H_2O colloidal dispersion), dimethyl sulfoxide (DMSO, ≥ 99.8%), N,N-dimethylformamide (DMF, ≥ 99.8%), and methylammonium iodide (CH_3NH_3I, MAI, ≥ 99.8%) were purchased from Alfa Aesar. Lead (II) iodide (PbI_2, ≥ 99.999%) and chlorobenzene (CB, ≥ 99.5%) were obtained from Sigma-Aldrich and Aladdin Reagent, respectively. Tungsten disulfide nanosheet powder (WS_2, average lateral size: ~ 100 nm) was purchased from Nanjing XFNANO Materials Co., Ltd. The 2,2',7,7'-tetrakis [N,N-di(4-meth-oxyphenyl)amino]-9,9'-spirobifluorene (spiro-OMeTAD, ≥ 99.0%), sulfonyl imide (Li-TFSI, ≥ 99%), acetonitrile (≥ 99.9%), and 4-tertbutylpyridine (TBP, ≥ 99%) were supplied by Yingkou Optimum Trade Co., Ltd. The purity of the silver (Ag) used for thermally evaporated electrode was 99.99%. All chemicals and reagents were directly used without further purification.

***Materials and devices characterization*:**

Transmission electron microscopy (TEM) images were taken using a JEOL-2010 TEM operating at a 200 kV accelerating voltage. The surface and cross-sectional morphologies of samples were measured using a field-emission scanning electron microscopy (SEM, JEOL, JSM-7800F). The material states of samples were characterized by means of Raman spectroscopy (Nanofinder 30, Tokyo Instruments Inc.), using laser excitation with a 514 nm wavelength. The optical properties, including transmission and absorption, were recorded on an UV−vis spectrophotometer (SHTMADZU, UV−3600plus). The relevant electrical parameters of different films were analyzed by a four-point probe system with a current source-

meter (RS8, BEGA Technologies). X-ray photoelectron spectroscopy (XPS) and ultraviolet photoelectron spectroscopy (UPS) were performed using an XPS/UPS system (Thermofisher, Excalab 250 xi). The chemical composition and state analysis of samples were measured by XPS, and the energy band structure was evaluated by UPS with the He I (21.22 eV) emission line employed for excitation. The surface potentials of films were measured with Kelvin probe force microscope (KPFM, Park Syetems NX20, Korea). The time-resolved photoluminescence (TRPL) spectrum was measured by a Fluorolog-3-TCSPC spectrometer (Edinburgh Instruments, FLS1000, UK). The electrochemical impedance spectroscopy (EIS) of solar cells was performed using an electrochemical workstation (CHI660C) at a voltage bias of 0.8 V in dark. The photocurrent density-voltage (J−V) curves of solar cells with different incident light directions were acquired using a solar simulator (Newport Oriel Solar 3A Class AAA) equipped with a 150−W xenon lamp under AM 1.5G (100 mW/cm^2) simulated sunlight. Light intensity was calibrated using a standard KG3-filtered silicon reference cell certified by the National Renewable Energy Laboratory. All devices were reverse scanned (from 1.2 V to – 0.2 V) at a scan rate of 130 mV/s, and the active area was delimited using the metal mask. The spectral response of devices was taken by an external quantum efficiency (EQE) measurement system (Newport, IQE 200^{TM}), equipped with a monochromator, a lock-in amplifier, a Xe lamp, and a current–voltage amplifier.